Journal of
Composites Science

MDPI

Article

Individual and Combined Effects of Reinforcements on Fractured Surface of Artificially Aged Al6061 Hybrid Composites

Manjunath Shettar, Sathyashankara Sharma, Gowrishankar M C *, Vishwanatha H M, Rakesh Ranjan and Srinivas Doddapaneni

Department of Mechanical and Industrial Engineering, Manipal Institute of Technology, Manipal Academy of Higher Education, Manipal 576104, India
* Correspondence: gowri.shankarmc@manipal.edu

Abstract: The present work mainly focuses on a comparative study of the individual and combined effect of reinforcements on tensile strength and fracture surface analysis of Al6061 alloy and its composites during artificial aging. SiC and B_4C are the two reinforcements used in the present work for the preparation of Al6061 composites by the stir casting process, and the reinforcement percentage from 2, 4, and 6 wt.% varied. Both Al6061 alloy and its composites are solution-treated at 558 °C/2 h and artificially aged at 100 and 200 °C for different time intervals to achieve peak aging. The results show substantial improvement in ultimate tensile strength during low temperature aging at 100 °C. Approximately 80–110% increase in UTS value is observed in both individual and hybrid composites compared to Al6061 alloy. The mechanism of failure governing the tensile strength for both alloy and its composites is thoroughly analyzed and discussed using a scanning electron microscope. The morphology of crack propagation is also studied to determine the mechanism of failure. Al6061 alloy shows ductile failure due to coarser dimples. Al6061-SiC composites show particle-matrix interface cracking and shear failure. Al6061-B_4C composites show elongated dimple rupture mode of failure, whereas Al6061-SiC + B_4C hybrid composites fail due to nucleation growth and mixed fracture mode.

Keywords: Al6061 alloy; boron carbide (B_4C); silicon carbide (SiC); hybrid composites; fractography

Citation: Shettar, M.; Sharma, S.; M C, G.; H M, V.; Ranjan, R.; Doddapaneni, S. Individual and Combined Effects of Reinforcements on Fractured Surface of Artificially Aged Al6061 Hybrid Composites. *J. Compos. Sci.* **2023**, *7*, 91. https://doi.org/10.3390/jcs7030091

Academic Editor: Francesco Tornabene

Received: 30 January 2023
Revised: 17 February 2023
Accepted: 28 February 2023
Published: 1 March 2023

1. Introduction

Aluminum (Al) alloy and its composites are available in a variety of alloy matrices, including Mg, Ti, and Al, with ceramic reinforcements in particulate, continuous fiber, or chopped fiber form. Al and its alloys have widely been utilized as the matrix in Al-based composites. B_4C and SiC are the most favored reinforcements for all these matrices, while other materials, such as Al_2O_3 and TiC, have been utilized in previous studies [1–5]. The size of the particles varies greatly between manufacturers and alloys; however, the average particulate size is often in the mm range. Steel and Al alloys have been widely used for fabrication in the automotive sector for many years and are now replaced by Al-based composites in many components (e.g., pistons, engine blocks, etc.) because of their good strength-to-weight ratio and excellent wear properties that are essential for critical automotive parts [6–10]. According to the extensive literature, boron carbide (B_4C) is an alternative for composites reinforced with silicon carbide (SiC) due to B_4C's superior interfacial bonding with matrix alloy. The interfacial bonding between the Al matrix and B_4C reinforcement is found to be better than that of SiC-reinforced composites [11–18]. The findings reveal that the composites' mechanical properties are greatly improved because of homogeneous reinforcement distribution and the establishment of an interface between the matrix and reinforcements. Compared to SiC-reinforced composites, B_4C-reinforced composites have greater strengthening effects. Shorowordi et al. [12] fabricated Al + SiC, Al + B_4C, and Al + Al_2O_3 composites using the stir casting method and compared their mechanical properties. The results conclude that the Al+B_4C composites displayed better

mechanical properties than the other two composites. Additionally, from fracture analysis it is concluded that better interfacial bonding took place in the Al+B_4C composites compared to Al +SiC and Al + Al_2O_3 composites. Auradi et al. [15] prepared Al6061 + B_4C composites using a conventional melt stirring process. Microstructural analysis confirms the homogenous distribution of reinforcement within the matrix. The presence of hard B_4C particles in Al 6061 matrix has improved the mechanical properties of prepared composites. Halil et al. [7] fabricated Al6061 hybrid composites using powder metallurgy with SiC and B_4C as reinforcements. From the morphological analysis, they conclude that agglomeration took place after 6 wt.% addition of B_4C, but the bonding between matrix and reinforcements is good. Additionally, the composites with higher wt.% of B_4C display better hardness values when compared to higher wt.% of SiC. The most common heat treatment procedure used to improve the specific strength of various Al alloys is age hardening [1,4,6,7,16–25]. The core objective of aging these alloys (Al-Mg-Si) is to produce many uniformly dispersed fine intermediate precipitates (Mg_2Si) in the matrix. Baradeshwaran and Elaya [13] fabricated Al7075 + B_4C composites using the casting technique and subjected the fabricated composites to T6 heat treatment. The results show that the heat-treated composites display better mechanical properties when compared to as-cast composites and alloys. The formation of hard intermetallic phases during T6 treatment is the major reason for improving the mechanical properties.

It is observed that minimal research is conducted on comparative study of fractured surfaces during the presence of individual and hybrid reinforcements on artificially aged Al6061 hybrid composites compared to as-cast Al6061 alloy. However, the literature review shows that there is a visible gap in exploring the improvement possibility in tensile properties of the hybrid composites by the careful selection of reinforcement combination. The novelty of the work is the substantial improvement in the tensile properties of the hybrid composites by selecting suitable pair and weight properties of reinforcement combination in the Al6061 matrix.

2. Matrix and Reinforcements Materials

In the current work, commercially procured Al6061 alloy is used as matrix material as per ES573(3)-2009, and its actual chemical composition is given in Table 1. On the other hand, the reinforcements that are used for composite preparation, viz., B_4C and SiC particles, are brought from "Boron Carbide India ltd", and "Indian Fine Chemicals", Mumbai, respectively. The properties of Al6061 alloy, SiC, and B_4C reinforcement particles are shown in Table 2.

Table 1. Chemical composition of Al6061 alloy.

Material	Mg	Si	Fe	Cr	Al
wt.% (Actual)	0.90	0.55	0.62	0.25	Bal.
wt.% (Standard)	0.8–1.2	0.4–0.8	0.7 max	0.35 max	Bal.

Table 2. Properties of Al6061 alloy, SiC, and B_4C reinforcements [14–18].

Properties	Al6061	SiC	B_4C
Poisson's Ratio	0.33	0.14	0.207
Size Range	-	30–40 μm	30–40 μm
Density (g/cm^3)	2.7	3.1	2.52
Hardness	30 BHN	28 GPa	30 GPa
Elastic Modulus (GPa)	70–80	410	480

The particle size of both B_4C and SiC reinforcements are in the range of 30–40 µm. To confirm the shape of the reinforcement particles, SEM analysis was carried out. From the SEM micrographs shown in Figure 1a,b, it is found that the particles are irregular in shape. The purity of powders is validated by x-ray diffraction (XRD) analysis, shown in Figure 1c,d.

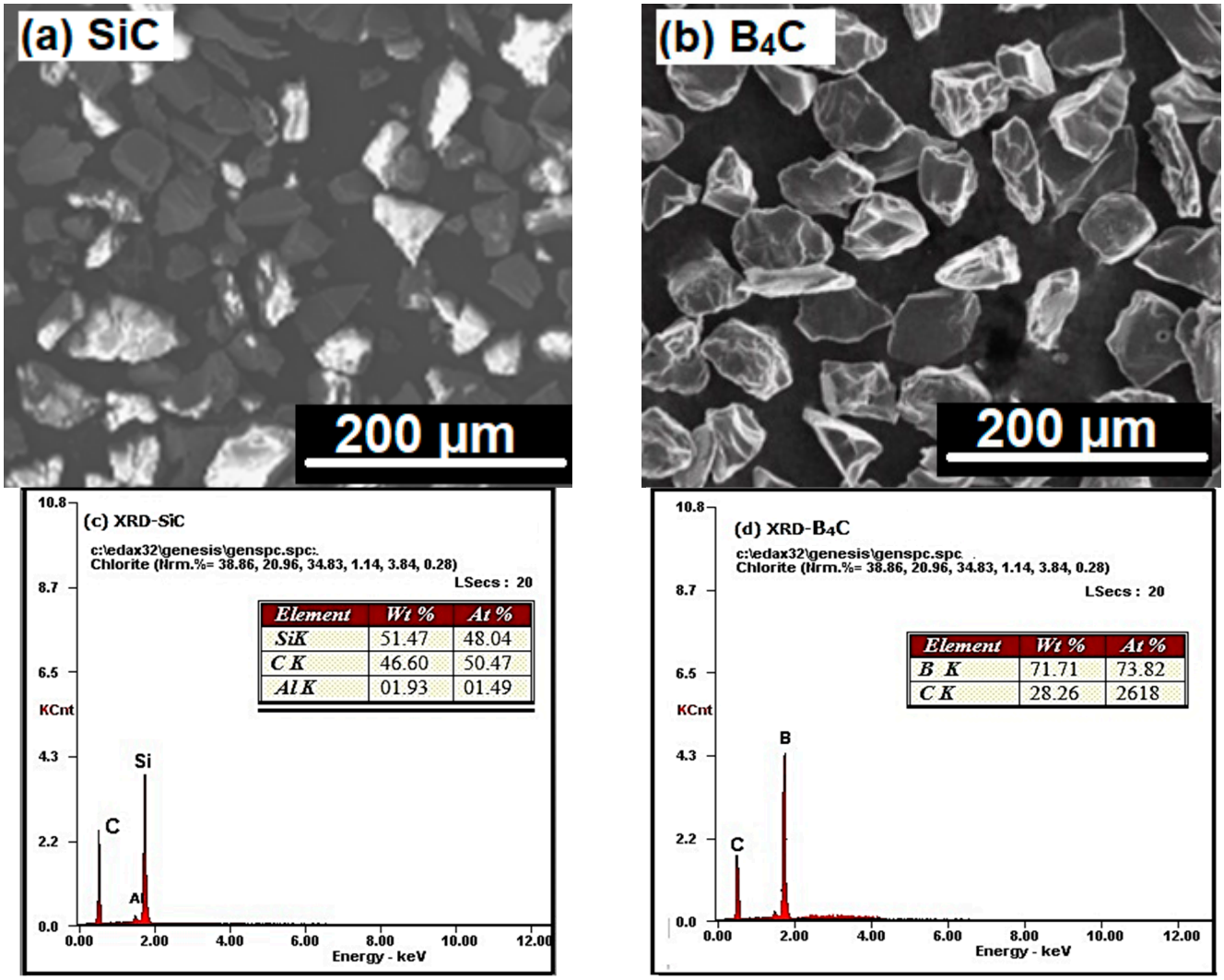

Figure 1. SEM micrographs (**a**,**b**) and corresponding XRD plots (**c**,**d**) of SiC and B_4C particles used in the present study.

3. Processing of Al6061 Metal Matrix Composites (MMCs)

The various MMCs studied in the present work are synthesized using the stir casting technique, and the experimental setup used in the present work is shown in Figure 2. The setup consists of a custom-made electric furnace and an electric stirrer mounted on top of the furnace. Initially, Al6061 alloy is taken in a graphite crucible, the furnace is switched on, and the temperature is gradually raised to 750 °C. Once the alloy is melted in the crucible, scum powder is added, and slag is removed. The liquid melt is degassed using Hexa Chloroethane (C_2Cl_6, 0.3 wt.%) tablet [26–28]. The temperature of the melt is reduced to 600 °C, a stirrer is introduced into the crucible containing semisolid Al6061 alloy, and a stirring speed of 150–200 rpm for 10 min is maintained to create a vortex and obtain uniform dispersion of reinforcement particles in the Al6061 matrix [29–31]. The calculated amount of preheated reinforcement powder is slowly introduced into the vortex at this stage.

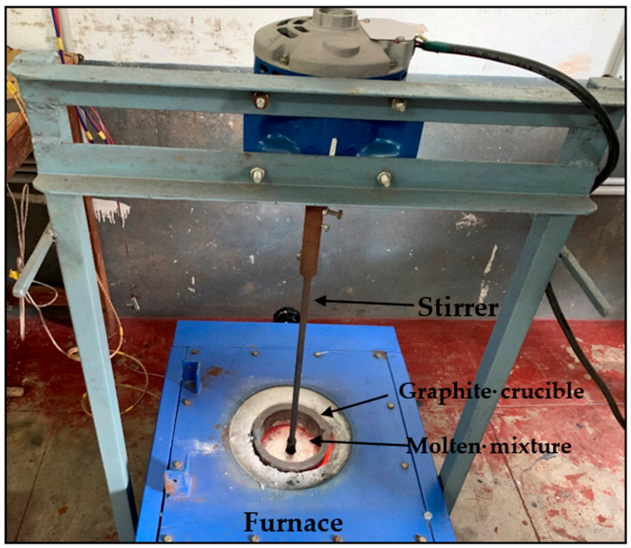

Figure 2. Stir casting experimental setup used in the current study.

In all three cases, i.e., after adding SiC, B_4C, and SiC + B_4C together to the Al melt in the semisolid state, the composite slurry is re-heated to 750 ± 10 °C (above liquidus temperature), and stirring is continued for 10 min at a speed of 400 rpm. The molten mixture is poured into preheated moulds (made of cast iron) maintained at 500 °C. The molten mixture is allowed to solidify in the air. This process casts cylindrical tensile specimens. Three types of composites are fabricated in the present work, namely Al6061 + SiC, Al6061 + B_4C, and Al6061 + SiC + B_4C hybrid composites in three variants differing in the weight fraction of the reinforcements.

Before preheating, both SiC and B_4C particles are washed with distilled water in an ultrasonic agitator for 10–15 min. After each agitation, the water is decanted and replaced with new water. After washing the reinforcement particles with distilled water, ultrasonic agitation is used to clean them again with acetone. After that, the acetone is decanted, and the powder particles are dried.

To eliminate volatile compounds and keep the particle temperature near to Al6061 melt, SiC particles are preheated to 800 °C/2 h. The elimination of surface contaminants, the de-absorption of gases, and the creation of an oxide layer (SiO_2) on the surface all result from preheating the particles. This SiO_2 combines with the molten Al to generate the Al-Si-O compound, which increases the wettability of SiC with Al 6061 alloy [31–34].

In contrast, B_4C particles are preheated at 250 °C/2 h to eliminate volatile compounds. Preheating B_4C above 300 °C would result in reinforcement particle agglomeration and the production of a layer of boric oxide (B_2O_3). Preheating boron carbide particles removes surface contaminants and improves the wettability of the reinforcements [24,25].

Initially, Al6061 + SiC and Al6061 + B_4C composites are synthesized in three variants differing in weight fraction of the reinforcements with SiC and B_4C of 2, 4, and 6 wt.%. Hybrid composites are also prepared in the proportion of boron carbide (1, 2, and 3 wt.%) and silicon carbide powder mixture in varying proportions (5, 4, and 3 wt.%) which are designated with the different notations shown in Table 3. The total quantity of the reinforcements in all three hybrid composites is restricted to 6 wt.% (1B5S, 2B4S, and 3B3S) to avoid agglomeration and inappropriate distribution of reinforcements during stirring.

Table 3. Al6061 hybrid composites with different proportions of SiC and B_4C reinforcements.

	wt.% of SiC and B_4C with Al 6061 Alloy
1B5S	Al6061 + B_4C (1 wt.%) + SiC (5 wt.%)
2B4S	Al6061 + B_4C (2 wt.%) + SiC (4 wt.%)
3B3S	Al6061 + B_4C (3 wt.%) + SiC (3 wt.%)

4. Characterization of Al6061 Alloy and Composites Tensile Test Specimen

The tensile test samples are prepared as per the ASTM-E8M standard, as indicated in Figure 3, with a 6 mm diameter cross-section and a gauge length of 24 mm. For each composition, five tensile test specimens are prepared and tested using an electronic tensometer; the average of five test results is considered, and the standard deviation is shown as error bars in the results. The load cell value is held constant at 20.5 kN, and the mode of the test is set to break. With a length increment value of 0.01 mm, the test speed is maintained uniformly at 10 mm/min. Actual machined tensile specimens as per ASTM standards are shown in Figure 4, and the specimens are identified with different color codes.

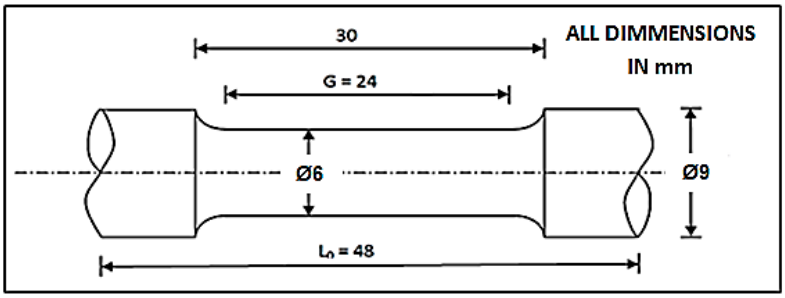

Figure 3. Tensile specimen as per ASTM-E8M.

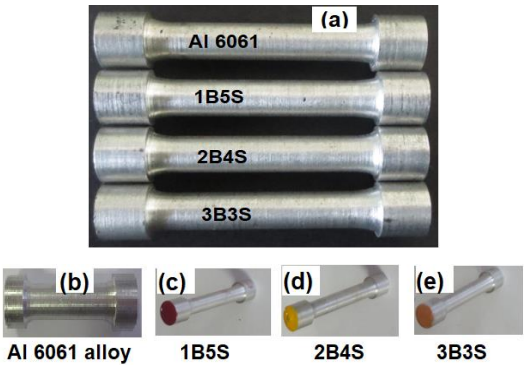

Figure 4. (**a**) Prepared tensile test specimen. (**b**) Al6061 alloy. (**c**) 1B5S, (**d**) 2B4S, (**e**) 3B3S composites.

The tensile test samples are now subjected to precipitation hardening treatment. During this heat treatment process, specimens are treated to solutionizing heat treatment, artificial aging, and quenching in water at room temperature. Specimens are soaked at 558 °C/2 h before being quenched in room temperature water. Melting of the ternary eutectic Mg_2Si-(Al)-(Mg) phase occurs at 558 °C, as per Al-Mg-Si phase diagram. Mg_2Si substantially enhances the strengthening effect; Mg_2Si dissolves fully at 558 °C during solutionizing and precipitates after age hardening. These subsequent precipitated stages further enhance the MMC. It has been observed that after aging, Al6061/SiC composite samples subjected to solution heat treatment at 558 °C display greater strength than samples solution-heat-treated at 530 °C [35].

The quenched specimens are transferred to furnaces maintained at 100 and 200 °C and are artificially aged for varying intervals of time until peak hardness is achieved. Peak hardness values obtained for both Al6061 alloy and its composites are already discussed in our previous work [4,5,15]. The optimum aging time to obtain peak hardness values during the age hardening process is shown in Table 4. Based on the peak-aged duration obtained from Table 4, tensile specimens are subjected to solutionizing and aging treatment with known duration before carrying out the tensile test. Scanning electron microscope (SEM-Model: JEOL JSM 840A) with energy dispersive x-ray (EDX) is used to analyze the mode of failure after the tensile test for Al6061 alloy and its composites.

Table 4. Peak aging time obtained during aging treatment after solutionizing treatment for Al6061 alloy and its composites [4,5,18].

Material	Peak Aging Time (h) for 100 & 200 °C
Al6061 alloy	12–15 h
Al6061 + SiC composites	6–10 h
Al6061 + B_4C composites	4–8 h
Al6061+ SiC + B_4C hybrid composites	2–6 h

5. Results and Discussion

5.1. Tensile Properties

The ultimate tensile strength (UTS) of the as-cast and peak-aged composites are displayed in Figures 5–7. The effect of adding SiC, B_4C, and SiC + B_4C reinforcements to Al6061 alloy is clearly observed. It is inferred that individual and hybrid composites display superior tensile strength compared to matrix alloy. The UTS of Al6061 alloy is 146 MPa, by adding reinforcements, the as-cast UTS of Al6061-SiC (6 wt.%), Al6061-B_4C (6 wt.%), and Al6061-3B3S MMCs measure 162, 176, and 201 MPa, respectively, and 10–40% increase in UTS value is observed for composites in as-cast condition over Al6061 alloy. It is observed from Figures 5 and 6 that the UTS of B_4C-reinforced composites is greater than SiC-reinforced composites. The addition of 6 wt.%. of SiC and B_4C individually on Al6061 alloy results in substantial improvement in UTS compared to 2 and 4 wt.% of SiC and B_4C. Similarly, in the case of hybrid composites, the addition of SiC and B_4C in equal proportions (3B3S) results in an appreciable increase in UTS. The presence of hard secondary phases on the soft matrix provides both grain size reduction and strengthening of the alloy, which improves mechanical properties even more [15,36–38].

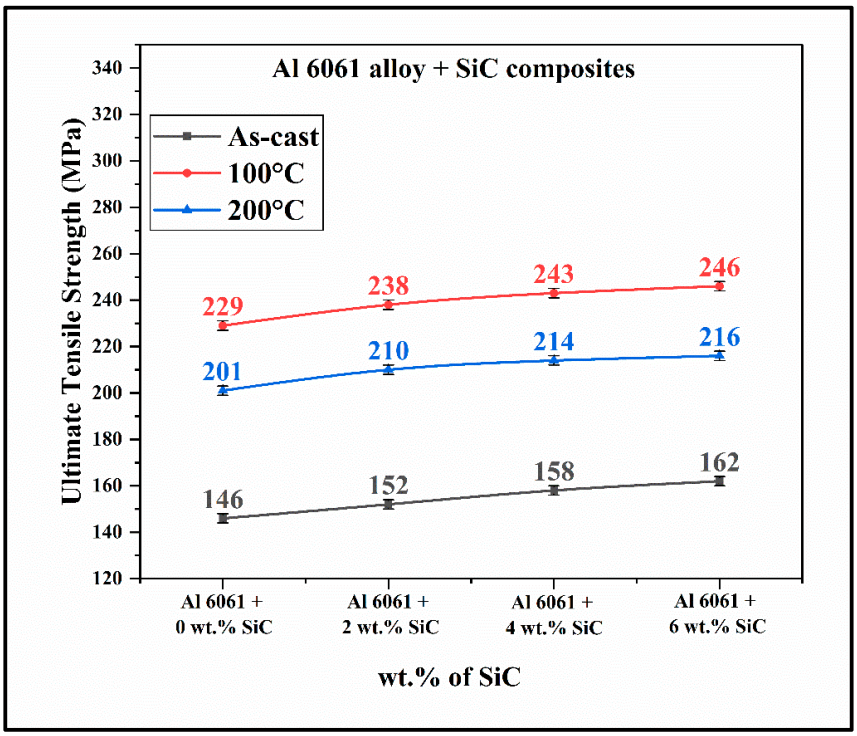

Figure 5. Variation of tensile strength with increase in content of SiC particles on Al 6061 alloy under different peak aging conditions.

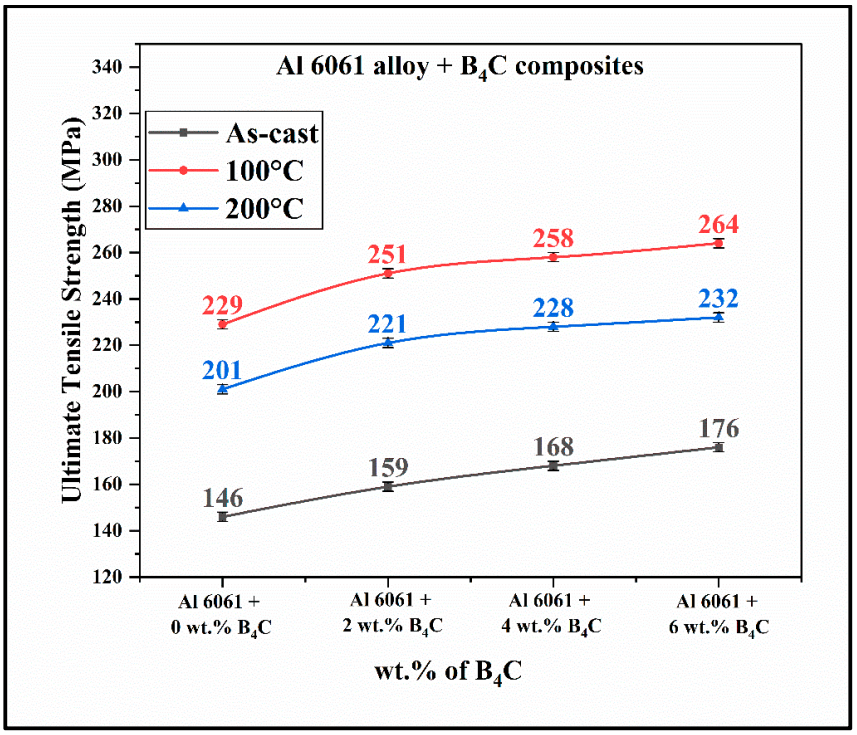

Figure 6. Variation of tensile strength with increase in content of B_4C particles on Al 6061 alloy under different peak aging conditions.

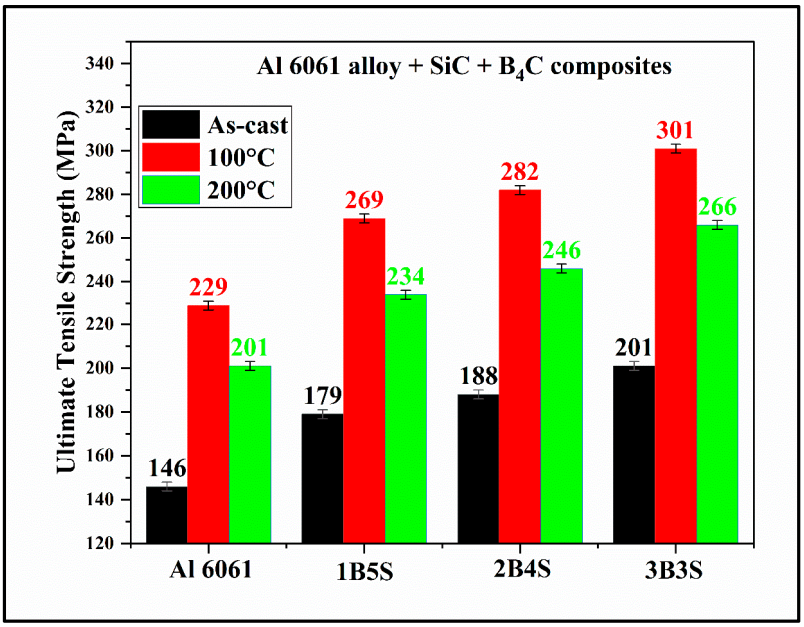

Figure 7. Variation of tensile strength with different quantity of SiC and B_4C particles on Al 6061 hybrid composites under different aging conditions.

As per our previous work [5,10,18,29–31], the uniform distribution of reinforcing particles is critical for advanced applications in the automobile and aerospace sectors. With a uniform distribution of reinforcements in the matrix and by attaining good interface bonding, the applied stress can be transmitted from the matrix to reinforcements with higher elastic modulus. With the inclusion of these ceramic particles (hard and high Young's modulus) into the matrix (toughness and ductility) results in a mixture of properties and generates a new set of better properties.

Al6061-B_4C composites show (Figure 6) higher UTS when compared to Al6061-SiC composites (Figure 5) for the same amount (2, 4, and 6 wt.%) of reinforcement. The increase in UTS may be due to the higher hardness of B_4C reinforcements, which contributes positively to alloy strengthening [38–43]. Similar observations are shown in 1B5S, 2B4S, and 3B3S hybrid composites (Figure 7). Improvement in tensile strength of hybrid composites can be traced to a greater degree to the formation of intermetallic precipitates [4,5], which function as impediments for pinning down dislocations and therefore limit the extent of plastic deformation.

Mohan et al. [39] noticed a similar behavior, wherein UTS increase is because of the presence of reinforcements acting as obstacles to the moving dislocations. The strengthening mechanism of Al6061 composites is mainly due to the load-bearing capacity of the reinforcements. Higher resistance to crack initiation and propagation can be achieved with better interaction between dislocations and reinforcements.

Higher dislocation density and dislocation particle interactions arise from higher particle concentration and lower aging temperature. When a load is applied, the presence of hard particles and intermetallics contribute to dislocation pileup, increased back stress, and work hardening (matrix) due to limited plastic flow in the ductile matrix. The synergistic impact of dislocation interaction with reinforcement, intermetallic, and grain boundaries contributes positively to alloy strengthening [8,29–31,40].

For the same amount (6 wt.%) of the reinforcements in Al6061 alloy with 1B5S, 2B4S, and 3B3S, substantial improvement in tensile strength is observed in Al6061-3B3S hybrid composite, as shown in Figure 7. This improvement is mainly due to the presence of harder reinforcement particles in the matrix and the effect of aging treatment. The graph shows that an increase in the wt.% of B_4C and lower aging temperature (100 °C) are favorable conditions for improved tensile strength in the hybrid composites. Improvement of UTS in composites during age hardening treatment compared to as-cast Al6061 alloy can be summarized as follows:

- 60–70% and 40–50% increase in peak-aged samples at 100 °C and 200 °C, respectively, for Al6061-SiC composites.
- 70–80% and 50–60% increase in peak-aged samples at 100 °C and 200 °C, respectively, for Al6061-B_4C composites.
- 85–110% and 60–80% increase in peak-aged samples at 100 °C and 200 °C, respectively, for hybrid composites.

Elongation percentage, which is the measure of ductility, is usually lower, and its value decreases with an increase in the amount of reinforcements in the case of Al alloy and its composites. The effective addition of SiC, B_4C, and SiC + B_4C results in an increase in UTS and decreases the ductility of composites. Figure 8a–c show the effect of SiC and B_4C reinforcement content on the percentage elongation in as-cast and lower temperature peak-aged (100 °C) conditions for both Al6061 alloy and its composites. The percentage elongation for Al6061-B_4C (Figure 8b)-reinforced composites is less compared to Al6061-SiC (Figure 8a)-reinforced composites. The reduction in percentage elongation is mainly due to an increase in the tensile strength of B_4C-reinforced composites.

Similar results are observed in hybrid composites, where the combined effect of SiC and B_4C decreases the percentage elongation in both as-cast and age-hardened conditions, as shown in Figure 8c. Quantitatively, a nearly 60–70% reduction in percentage elongation is observed with the increase in B_4C (1–3 wt.%). The hard B_4C and SiC reinforcements may produce embrittlement, resulting in localized stress concentration. These reinforcement particles prevent dislocation movement by either producing stress fields in the matrix or bringing substantial variations in the elastic behavior of the matrix and dispersoid [40].

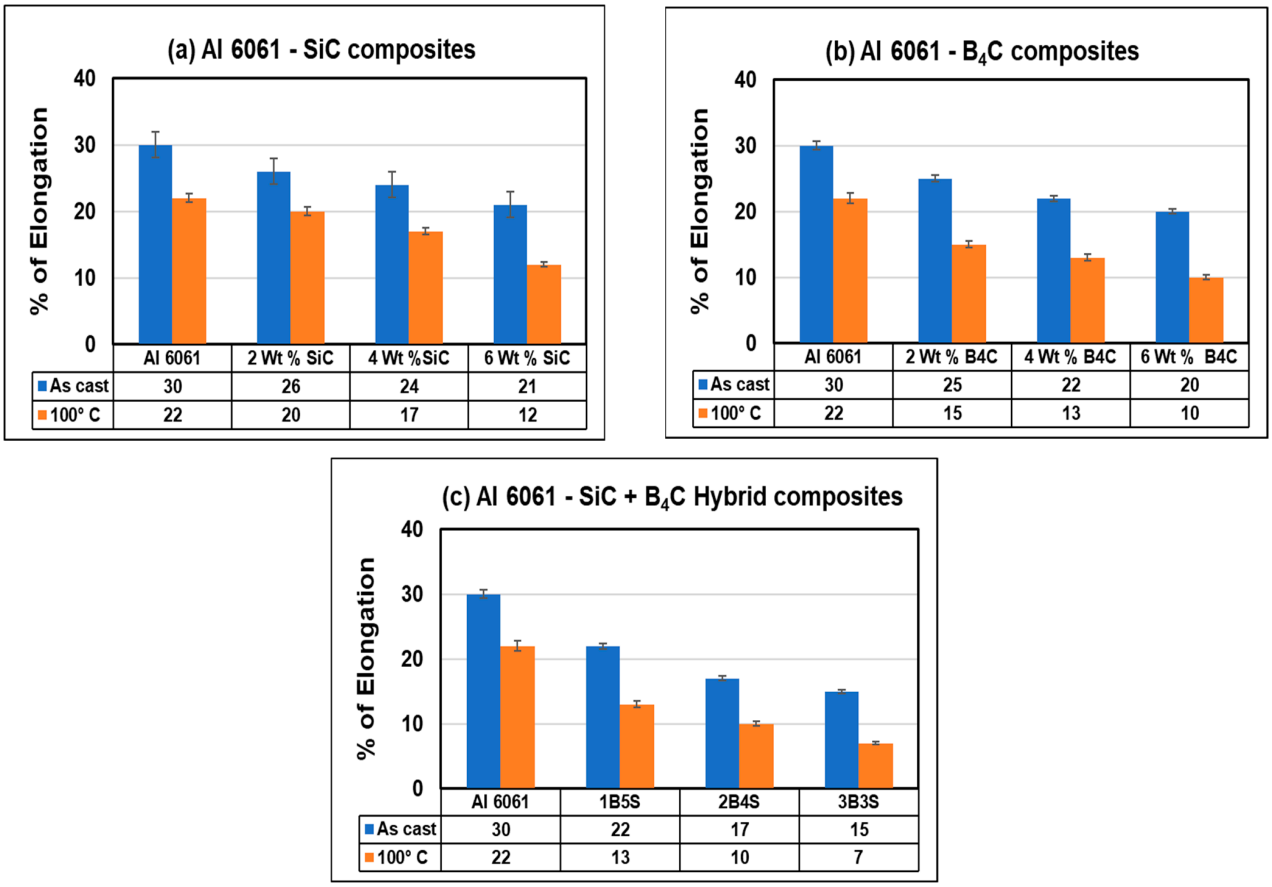

Figure 8. Effect of SiC and B_4C on percentage elongation of (**a**) Al6061-SiC, (**b**) Al6061-B_4C, and (**c**) Al6061-SiC + B_4C composites.

5.2. Fracture Surface Analysis of Al6061 Alloy and Its Composites

5.2.1. Al6061 Alloy

The fractured surface of the tensile tested specimen aged at 100 °C is examined through SEM, since Al6061 alloy, 6 wt.% SiC, 6 wt.% B_4C, and 3B3S composites aged at 100 °C show higher UTS. Fractography of Al6061 alloy (as-cast and peak-aged at 100 °C) are shown in Figure 9a–d. A colossal amount of fine cuplike equiaxial dimples are observed on the fractured surface and thus fracture mode is predominantly dimple rupture (Figure 9a,b). Several cuplike depressions are seen, which are referred to as dimple ruptures (Figure 9b). Some micro-voids are identified to grow near the grain boundary (GB) and other sites.

River pattern is regarded as the array of ultrafine to finer dimples present in thin strips, indicating that fracture is cleavage driven. At the same time, an enormous number of identical dimples are also observed, indicating higher ductility. Therefore, as-cast Al6061 alloy shows lower UTS and higher ductility. Figure 9c,d shows the fracture surface of peak-aged specimen (100 °C). In this condition, the dimples are finer in appearance and are densely formed and equally distributed, indicating the formation of more number of micro-voids at different locations.

The peak-aged specimen has smaller dimples on the fractured surface than the as-cast Al6061 alloy. The size of the dimple is directly proportional to strength and ductility. The finer the dimple size, the greater the ductility and strength of the joint and vice versa. As a result, the peak-aged specimen has greater UTS values than the as-cast Al6061 alloy [41,42].

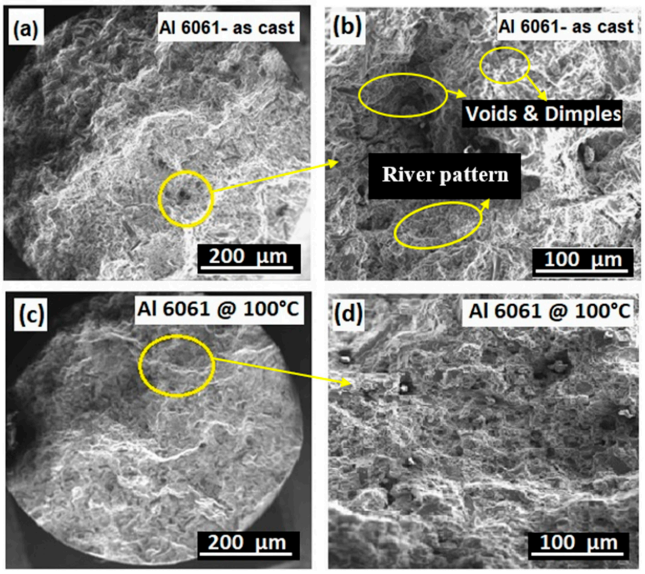

Figure 9. SEM fractographs of (**a**) as-cast Al6061 alloy (**b**) at higher magnification, (**c**) peak-aged sample at 100 °C, and (**d**) different locations at higher magnification.

5.2.2. Al6061-6 wt.% SiC Composites

Figure 10a–d depicts SEM images of the fractured surface of tensile test composite specimens in as-cast and peak-aged at 100 °C with 6 wt.% SiC. The overall fracture mode is mixed (ductile and brittle). Fractography reveals exposed SiC on the fracture surface, showing that MMCs fail primarily via the matrix (Figure 10a,b). Furthermore, as displayed in Figure 10c,d, tested composites fail in a few spots due to particle/matrix interface breakage. The primary cause of fractures is poor interface bonding and void propagation. This is mostly due to strain localization at the SiC particles' sharp edges. These voids are subsequently merged during tensile stress, resulting in void coalescence and the production of fractures, which leads to void nucleation growth (VNG) failure at the fracture surface. The presence of a reasonably smooth fracture surface suggests ductile failure. Furthermore, the presence of furrows or a linear mark pattern in the crack propagation zone shows the attainment of peak aging (Figure 10d), resulting in an improvement in UTS [43,44].

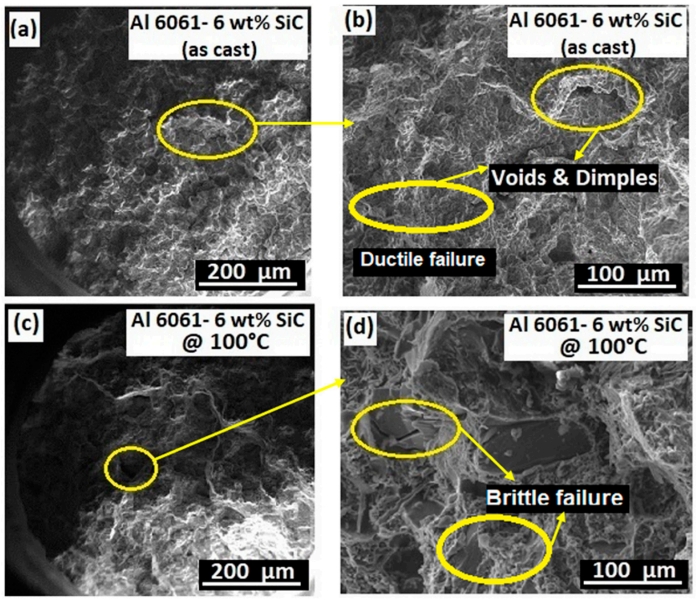

Figure 10. SEM fractographs of as-cast (**a**) Al6061-6 wt.%. SiC composite (**b**) at higher magnification. (**c**) Al6061-6 wt.% SiC composite peak-aged at 100 °C. (**d**) Different locations at higher magnification.

5.2.3. Al6061-6 wt.% B_4C Composites

Figure 11a,b illustrate the fractured surface of the as-cast composite Al6061-6 wt.% B_4C, which displays a lower density of dimples compared to the Al6061 and Al6061-SiC composites. Fractures in a confined area could be due to rip or shear, resulting in elongated dimples, and some shallow dimples could be caused by the shear-induced coalescence of micro voids, as shown in Figure 11a,b.

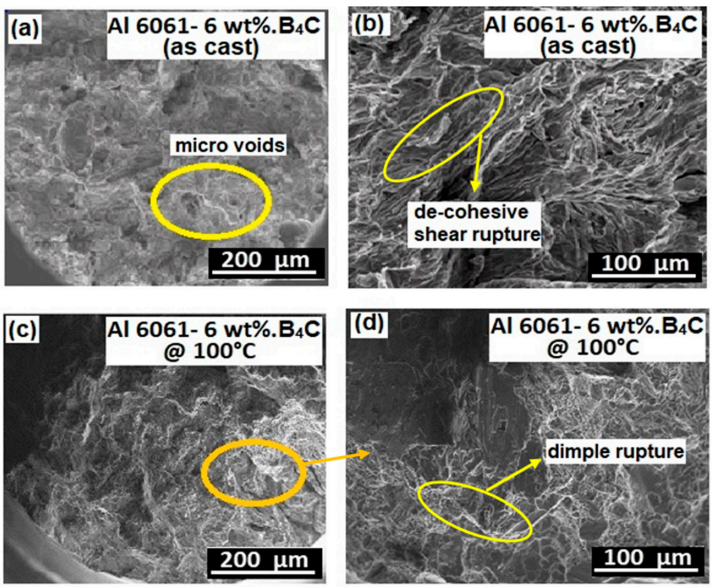

Figure 11. SEM fractographs of as-cast (**a**) Al6061-6 wt.%. B_4C composite (**b**) at higher magnification. (**c**) Al6061-6 wt.% B_4C composite peak-aged at 100 °C. (**d**) Different locations at higher magnification.

For the peak-aged sample at 100 °C depicted in Figure 11c,d, dimple rupture is the fracture mechanism. Dimples are formed due to the stimulation of multiple nucleation sites, leading to the development of micro-voids and their subsequent coalescence. In some regions, there is evidence of quasi-cleavage fractures, which is confined and exhibits characteristics of cleavage and plastic deformation, as shown in Figure 11c. In a few areas (Figure 11d), dimples appear elongated and depend on loading conditions. Localized fractures may be due to a tear or shear, resulting in elongated dimples, while shallow dimples are similar to those observed in Al6061-6 wt.% SiC composites.

Figure 11b shows a de-cohesive rupture caused by the rupture of protective films around B_4C. Whereas, Figure 11d indicates that the density of voids increases with an increase in the wt.% of B_4C, which acts as a nucleation site for voids, leading to the production of fractures and dimple fractures. The level of stress within the material governs the creation of dimples. Figure 11c,d reveal the existence of dendritic nodules inside a typical shrinkage cavity, which initiates failure, and crack propagation primarily happens through interdendritic separation, as reported in [45–51].

5.2.4. Al6061-SiC + B_4C Hybrid Composites

Fracture analysis is usually beneficial in understanding microstructural influence on tensile properties. Generally, HMMCs are usually brittle when compared to their alloy counterparts. Dimple rupture is connected with fracture advancement due to void nucleation and subsequent growth. The fracture process may alter significantly when ceramic reinforcements are introduced. Apart from the production of voids, coalescence, and shear crash in the matrix, this micro-mechanism might be caused by particle fracture, de-bonding, or cracking along the interface.

Figure 12a,b depicts the fractography of as-cast hybrid composites at lower and higher magnifications. The fractured surface has virtually identical characteristics. Fracture surfaces appear to be quite bumpy. On the surface, there is also evidence of porosity. The

presence of harder reinforcements and river-like patterns in some places is also observed, indicating ductile failure. The mode of fracture is clearly dimple rupture as a result of micro-void nucleation, growth, and coalescence. It is also noted that the type of fracture is caused by matrix failure by shear.

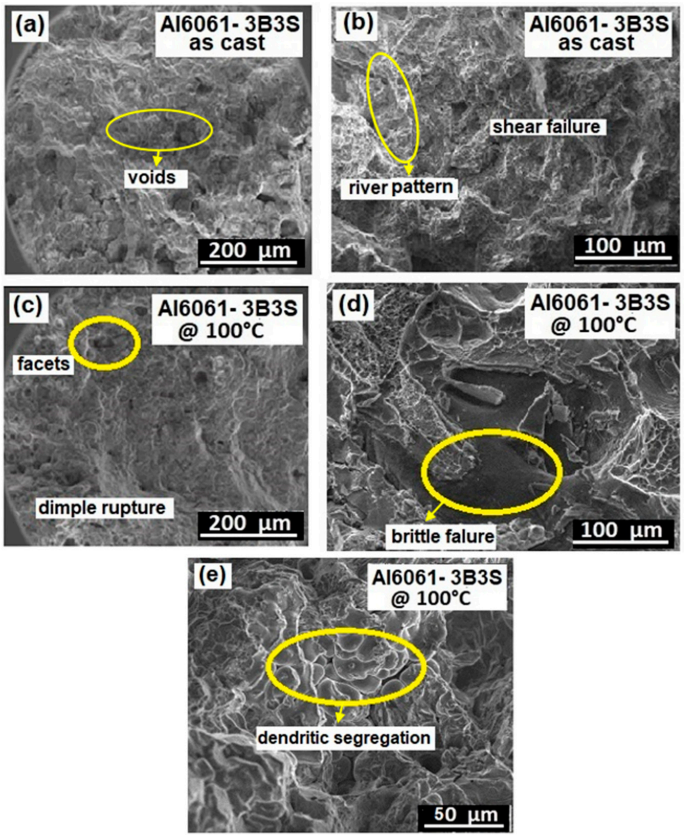

Figure 12. SEM fractographs of as-cast (**a**) Al6061-3B3S hybrid composite (**b**) at higher magnification. (**c**) Al6061-3B3S hybrid composite peak-aged at 100 °C. (**d**,**e**) Different locations at higher magnification.

Figure 12c–e depicts the fractured surface of tensile specimens of the tested hybrid composites at peak aging (100 °C). Excellent UTS and reduced ductility of Al6061-3B3S indicate greater bonding. Figure 12c depicts lower-density micro-voids in the fracture surface at the particle/matrix interface. As demonstrated in Figure 12d,e, the inclusion of tougher reinforcing particles causes shrinkage voids owing to coarser interdendritic segregation, which can lead to brittle failure. The presence of facets, the mirror surface, and the river pattern is evidence of mixed mode (brittle and ductile) failure (Figure 12c–e).

The important criterion for determining the fracture mode of composites is the connection between matrix strength and particle/matrix interfacial bond strength. Particle fracture generally happens during the permanent deformation stage if the particle/matrix interfacial connection is strong. If particle/matrix interfacial interaction is weak, decohesion occurs between particles and matrix prior to particle breakage.

6. Conclusions

The stir-cast Al6061 alloy reinforced with SiC/B_4C/SiC + B_4C composites was successfully fabricated using a two-step stir casting technique, subjected to precipitation hardening treatment, and further tested for tensile properties. The present study clearly shows that there is substantial improvement in the ultimate tensile strength. The tensile property trend in the reinforcement type and quantity change is in line with the peak hardness trend. An increase in 40–80% and 60–110% in UTS is observed during the peak aging of individual and hybrid-reinforced composites. The fracture mode of Al6061 alloy is predominantly dimple rupture. Peak-aged tensile fracture surfaces of base alloy exhibit the

mixed mode of failure. The fracture surface of SiC-reinforced composite shows improper interface bonding, and the mode of fracture is dimple rupture due to micro-void nucleation, growth, and coalescence. Fracture surface analysis indicates the shear failure of the matrix. The B_4C-reinforced composite fracture surface shows quasi-cleavage fractures and plastic deformation. The fracture of Al6061-SiC + B_4C hybrid composites shows dimple rupture due to micro-void nucleation, growth, and coalescence, where the cleavage mode of failure is prominent.

Author Contributions: Conceptualization, S.S. and G.M.C.; methodology, G.M.C., V.H.M., M.S., S.S. and R.R; investigation, M.S., R.R. and G.M.C.; data curation, M.S., V.H.M. and S.D.; writing—original draft preparation, S.S. and G.M.C.; writing—review and editing, M.S., G.M.C. and S.S.; supervision, S.S.; project administration, S.S., M.S. and G.M.C. All authors have read and agreed to the published version of the manuscript.

Funding: This research received no external funding.

Data Availability Statement: Not applicable.

Acknowledgments: The authors would like to acknowledge Manipal Academy of Higher Education, Manipal for providing the infrastructural facility to conduct the experimental works.

Conflicts of Interest: The authors declare no conflict of interest.

References

1. Robledo, J.D.E.; Shetty, P.; Kumari, P.P.; Shankar, M.C.G.; Kagatikar, S. Gravimetric, electrochemical and theoretical study on corrosion of AA6061/3wt.% SiC/3wt.% B_4C hybrid composite in acid medium using EDTA. *Tribol. Ind.* **2022**, *44*, 73–86. [CrossRef]
2. Nithesh, K.; Gowri Shankar, M.C.; Nayak, R.; Sharma, S.S. Effect of light weight reinforcement and heat treatment process parameters on morphological and wear aspects of hypoeutectic Al-Si based composites—A critical review. *J. Mater. Res. Technol.* **2021**, *15*, 42724292. [CrossRef]
3. Jayashree, P.K.; Gowri Shankar, M.C.; Sharma, S.S.; Shetty, R.; Hiremath, P.; Shettar, M. The effect of SiC content in aluminum-based metal matrix composites on the microstructure and mechanical properties of welded joints. *J. Mater. Res. Technol.* **2021**, *12*, 2325–2339. [CrossRef]
4. Sharma, S.S.; Gurumurthy, B.M.; Gowri Shankar, M.C.; Kini, A.U.; Shettar, M.; Hiremath, P. Aging kinetics and microstructural features of Al6061-SiC+B_4C stir cast hybrid composites. *Int. J. Automot. Mech. Eng.* **2019**, *16*, 7211–7224. [CrossRef]
5. Gowri Shankar, M.C.; Sharma, S.S.; Kini, A.U.; Jayashree, P.K.; Gurumurthy, B.M. Study of wear behavior and mechanical mixed layer on artificial aged Al6061 composite reinforced with B_4C particles. *Indian J. Sci. Technol.* **2016**, *9*, 12. [CrossRef]
6. Sharma, S.; Singh, J.; Gupta, M.K.; Mia, M.; Dwivedi, S.P.; Saxena, A.; Chattopadhyaya, S.; Singh, R.; Pimenov, D.Y.; Korkmaz, M.E. Investigation on mechanical, tribological and microstructural properties of Al-Mg-Si-T6/SiC/muscovite-hybrid metal-matrix composites for high strength applications. *J. Mater. Res. Technol.* **2021**, *12*, 1564–1581. [CrossRef]
7. Halil, K.; İsmail, O.; Sibel, D.; Ramazan, Ç. Wear and mechanical properties of Al6061/SiC/B_4C hybrid composites produced with powder metallurgy. *J. Mater. Res. Technol.* **2019**, *8*, 5348–5361. [CrossRef]
8. Ahn, H.K.; Yu, C.H. Effect of SiC volume fraction on the age-hardening behavior in SiC particulate-reinforced 6061 aluminum alloy composites. *Met. Mater. Int.* **2001**, *7*, 1–7. [CrossRef]
9. Alaneme, K.K.; Aluko, A.O. Fracture toughness and tensile properties of as-cast and age-hardened aluminium (6063)–silicon carbide particulate composites. *Sci. Iran.* **2012**, *19*, 992–996. [CrossRef]
10. Gowri Shankar, M.C.; Achutha, K.; Sharma, S.S.; Prabhu, P.R. Influence of aging temperature and aging time on the mechanical property and microstructure during precipitation hardening of Al6061 alloy. *Int. J. Appl. Eng. Res.* **2015**, *10*, 25–31.
11. Kumar, M.S.; Vasumathi, M.; Begum, S.R.; Luminita, S.M.; Pruncu, C.I. Influence of B_4C and industrial waste fly ash reinforcement particles on the micro structural characteristics and mechanical behavior of aluminium (Al–Mg–Si-T6) hybrid metal matrix composite. *J. Mater. Res. Technol.* **2021**, *15*, 1201–1216. [CrossRef]
12. Shorowordi, K.M.; Laoui, T.; Haseeb, A.S.M.A.; Celis, J.P.; Froyen, L. Microstructure and interface characteristics of B_4C, SiC and Al_2O_3 reinforced Al matrix composites: A comparative study. *J. Mater. Process. Technol.* **2003**, *142*, 738–743. [CrossRef]
13. Baradeswaran, A.; Elaya Perumal, A. Influence of B_4C on the tribological and mechanical properties of Al 7075–B_4C composites. *Compos. Part B Eng.* **2013**, *54*, 146–152. [CrossRef]
14. Chen, X.; Fu, D.; Teng, J.; Zhang, H. Hot deformation behavior and mechanism of hybrid aluminum-matrix composites reinforced with micro-SiC and nano-TiB_2. *J. Alloys Compd.* **2018**, *753*, 566–575. [CrossRef]
15. Auradi, V.; Rajesh, G.L.; Kori, S.A. Processing of B_4C particulate reinforced 6061aluminum matrix composites by melt stirring involving two-step addition. *Procedia Mater. Sci.* **2014**, *6*, 1068–1076. [CrossRef]
16. Byeongyun, J.; Simanta, L.; Qi, A.; Madhav, R. Mechanical properties and deformation behavior of superhard lightweight nonocrystalline ceramics. *Nanomaterials* **2022**, *12*, 3228. [CrossRef]

17. Velavan, K.; Palanikumar, K.; Natarajan, E.; Lim, W.H. Implications on the influence of mica on the mechanical properties of cast hybrid (Al+10%B_4C+Mica) metal matrix composite. *J. Mater. Res. Technol.* **2021**, *10*, 99–109. [CrossRef]
18. Gowri Shankar, M.C.; Shettar, M.; Sharma, S.S.; Kini, A.U.; Jayashree, P.K. Enhancement in hardness and influence of artificial aging on stir cast Al6061-B_4C and Al6061-SiC composites. *Mater. Today Proc.* **2018**, *5*, 2435–2443. [CrossRef]
19. Kumar, J.; Singh, D.; Kalsi, N.S.; Sharma, S.; Pruncu, C.I.; Pimenov, D.Y. Comparative study on the mechanical, tribological, morphological and structural properties of vortex casting processed, Al-SiC-Cr hybrid metal matrix composites for high strength wear-resistant applications: Fabrication and characterizations. *J. Mater. Res. Technol.* **2020**, *9*, 13607–13615. [CrossRef]
20. Kumar, J.; Singh, D.; Kalsi, N.S.; Sharma, S.; Mia, M.; Singh, J.; Rahman, M.A.; Khan, A.M.; Rao, K.V. Investigation on the mechanical, tribological, morphological and machinability behavior of stir-casted Al/SiC/Mo reinforced MMCs. *J. Mater. Res. Technol.* **2021**, *12*, 930–946. [CrossRef]
21. Gopal Krishna, U.B.; Sreenivas Rao, K.V.; Vasudeva, B. Effect of percentage reinforcement of B_4C on the tensile property of aluminium matrix composites. *Int. J. Mech. Eng. Robot. Res.* **2012**, *1*, 290–295.
22. Hashim, J.; Looney, L.; Hashmi, M.S.J. Metal matrix composites: Production by the stir casting method. *J. Mater. Process. Technol.* **1999**, *92*, 1–7. [CrossRef]
23. Hashim, J.; Looney, L.; Hashmi, M.S.J. Particle distribution in cast metal matrix composites-Part-I. *J. Mater. Process. Technol.* **2002**, *123*, 251–257. [CrossRef]
24. Kalaiselvan, K.; Murugan, N.; Parameswaran, S. Production and characterization of AA6061-B_4C stir cast composite. *Mater. Des.* **2011**, *32*, 4004–4009. [CrossRef]
25. Mahesh, V.P.; Nair, P.S.; Rajan, T.P.D.; Pai, B.C.; Hubli, R.C. Processing of surface treated boron carbide-reinforced aluminium matrix composites by liquid-metal stir-casting technique. *J. Compos. Mater.* **2011**, *45*, 2371–2378. [CrossRef]
26. Previtali, B.; Pocci, D.; Taccardo, C. Application of traditional investment casting process to aluminium matrix composites. *Compos. Part A Appl. Sci. Manuf.* **2008**, *39*, 1606–1617. [CrossRef]
27. Singh, V. *Heat Treatment of Metals*; Standard Publishers Distributors: Delhi, India, 2012; pp. 521–535.
28. John, E.G. *The Treatment of Liquid Aluminium and Silicon Alloys*; American Foundrymen's Society: Schaumburg, IL, USA, 1990; pp. 172–175.
29. Gowri Shankar, M.C.; Achutha, K.; Sharma, S.S.; Prabhu, P.R. Effect of SiC particulate reinforcement on the precipitation hardening behavior of two step stir cast Al 6061 alloy. *Int. J. Appl. Eng. Res.* **2015**, *10*, 18–24.
30. Gowri Shankar, M.C.; Jayashree, P.K.; Achutha, K.; Sharma, S. Effect of precipitation hardening on stir cast Al 6061-B_4C reinforced composite. *Int. J. Mech. Prod. Eng. Res. Dev.* **2018**, *8*, 459–466.
31. Sharma, S.S.; Gowri Shankar, M.C.; Achutha, K. Metallographic and Bulk Hardness of Artificially Aged Al6061-B_4C-SiC Stir Cast Hybrid Composites. *J. Sci. Ind. Res.* **2017**, *880*, 140–143. [CrossRef]
32. Urena, A.; Martınez, E.E.; Rodrigo, P.; Gil, L. Oxidation treatments for SiC particles used as reinforcement in aluminium matrix composites. *Compos. Sci. Technol.* **2004**, *64*, 1843–1854. [CrossRef]
33. Kumar, G.V.; Rao, C.S.P.; Selvaraj, N. Studies on mechanical and dry sliding wear of Al6061–SiC composites. *Compos. Part B Eng.* **2012**, *43*, 1185–1191. [CrossRef]
34. Rashnoo, K.; Sharifi, M.J.; Azadi, M.; Azadi, M. Influences of reinforcement and displacement rate on microstructure, mechanical properties and fracture behaviors of cylinder-head aluminum alloy. *Mater. Chem. Phys.* **2020**, *255*, 123441. [CrossRef]
35. Rajasekaran, S.; Udayashankar, N.K.; Nayak, J. T4 and T6 treatment of 6061 Al-15 vol.% SiC_P composite. *ISRN Mater. Sci.* **2012**, *2012*, 374719. [CrossRef]
36. Ibrahim, M.F.; Ammar, H.R.; Samuel, A.M.; Soliman, M.S.; Almajid, A.; Samuel, F.H. Mechanical properties and fracture of Al–15 vol.% B_4C based metal matrix composites. *Int. J. Cast Met. Res.* **2014**, *27*, 7–14. [CrossRef]
37. Nie, C.-Z.; Gu, J.-J.; Liu, J.-L.; Zhang, D. Production of boron carbide reinforced 2024 aluminum pmatrix composites by mechanical alloying. *Mater. Trans.* **2007**, *48*, 990–995. [CrossRef]
38. Milan, M.T.; Bowen, P. Tensile and fracture toughness properties of SiC_p reinforced Al alloys: Effects of particle size, particle volume fraction, and matrix strength. *J. Mater. Eng. Perform.* **2004**, *13*, 775–783. [CrossRef]
39. Mohan, V.; Kori, S.A.; Sridhar, B.R.; Padasalgi, S.B. Synthesis and characterization of aluminium alloy A356 and silicon carbide metal matrix composite. In Proceedings of the 2nd International Conference on Industrial Technology and Management, Phuket Island, Thailand, 1–2 September 2012; IPCIT: Singapore, 2012; Volume 49, pp. 11–15.
40. Jameel Habeeb, G. Influence of ceramic particles reinforcement on some mechanical properties of AA 6061 aluminium alloy. *Eng. Technol. J.* **2013**, *31*, 2611–2618.
41. Mrówka, N.; Sieniawski, J.; Nowotnik, A. Tensile properties and fracture toughness of heat treated 6082 alloy. *J. Achiev. Mater. Manuf. Eng.* **2006**, *17*, 105–108.
42. Siddiqui, R.A.; Abdul-Wahab, S.A.; Pervez, T. Effect of aging time and aging temperature on fatigue and fracture behavior of 6063 aluminum alloy under seawater influence. *Mater. Des.* **2008**, *29*, 70–79. [CrossRef]
43. Ehsani, R.; Reihani, S.S. Aging behavior and tensile properties of squeeze cast Al6061/SiC metal matrix composites. *Sci. Iran.* **2004**, *11*, 392–397.
44. Mahadevan, K.; Raghukandan, K.; Pai, B.C.; Pillai, U.T.S. Experimental investigation on the influence of reinforcement and precipitation hardening parameters of AA 6061-SiC_p composites. *Indian J. Eng. Mater. Sci.* **2007**, *14*, 277–281.

45. Herbert, M.A.; Das, G.; Maiti, R.; Chakraborty, M.; Mitra, R. Tensile properties of cast and mushy state rolled Al-4.5Cu alloy and in situ Al4.5Cu-5TiB_2 composite. *Int. J. Cast Met. Res.* **2015**, *23*, 216–224. [CrossRef]
46. Tang, S.; Shao, S.; Liu, H.; Jiang, F.; Fu, D.; Zhang, H.; Teng, J. Microstructure and mechanical behaviors of 6061 Al matrix hybrid composites reinforced with SiC and stainless steel particles. *Mater. Sci. Eng. A* **2020**, *804*, 140732. [CrossRef]
47. Li, L.; Chen, B.; Que, L.; Zhao, G. Fabrication and strengthening mechanism of dual-phased and bimodal-sized (Si_3N_4 + TiB_2)/6061Al hybrid composite. *Mater. Des.* **2022**, *220*, 110872. [CrossRef]
48. Rezaei, M.R.; Albooyeh, A.; Shayestefar, M.; Shiraghaei, H. Microstructural and mechanical properties of a novel Al-based hybrid composite reinforced with metallic glass and ceramic particles. *Mater. Sci. Eng. A* **2020**, *786*, 139440. [CrossRef]
49. Doddapaneni, S.; Kumar, S.; Shettar, M.; Rao, S.; Sharma, S.; MC, G. Experimental investigation to confirm the presence of TiB_2 reinforcements in the matrix and effect of artificial aging on hardness and tensile properties of stir-cast LM4-TiB_2 composite. *Crystals* **2022**, *12*, 1114. [CrossRef]
50. Srinivas, D.; Shankar, G.; Sharma, S.; Kini, A.; Shettar, M. Effects of solutionizing and aging alteration on tensile behavior of stir cast LM4-Si_3N_4 composites. *Int. J. Automot. Mech. Eng.* **2022**, *19*, 4. [CrossRef]
51. David Raja, J.; Dinaharan, I.; Vibin, S.P.; Mashinini, P.M. Microstructure and mechanical characterization of in situ synthesized AA6061/(TiB_2+Al_2O_3) hybrid aluminum matrix composites. *Int. J. Automot. Mech. Eng.* **2018**, *740*, 529–535. [CrossRef]